JBC RESEARCH ARTICLE

Disturbed intramitochondrial phosphatidic acid transport impairs cellular stress signaling

Received for publication, November 4, 2020, and in revised form, January 11, 2021 Published, Papers in Press, January 23, 2021,
https://doi.org/10.1016/j.jbc.2021.100335

Akinori Eiyama[1], **Mari J. Aaltonen**[2], **Hendrik Nolte**[1], **Takashi Tatsuta**[1], **and Thomas Langer**[1,2,*]

From the [1]*Max-Planck-Institute for Biology of Ageing, Cologne, Germany; and* [2]*Cologne Excellence Cluster on Cellular Stress Responses in Aging-Associated Diseases (CECAD), University of Cologne, Cologne, Germany*

Edited by Dennis Voelker

Lipid transfer proteins of the Ups1/PRELID1 family facilitate the transport of phospholipids across the intermembrane space of mitochondria in a lipid-specific manner. Heterodimeric complexes of yeast Ups1/Mdm35 or human PRELID1/TRIAP1 shuttle phosphatidic acid (PA) mainly synthesized in the endoplasmic reticulum (ER) to the inner membrane, where it is converted to cardiolipin (CL), the signature phospholipid of mitochondria. Loss of Ups1/PRELID1 proteins impairs the accumulation of CL and broadly affects mitochondrial structure and function. Unexpectedly and unlike yeast cells lacking the CL synthase Crd1, Ups1-deficient yeast cells exhibit glycolytic growth defects, pointing to functions of Ups1-mediated PA transfer beyond CL synthesis. Here, we show that the disturbed intramitochondrial transport of PA in *ups1*Δ cells leads to altered unfolded protein response (UPR) and mTORC1 signaling, independent of disturbances in CL synthesis. The impaired flux of PA into mitochondria is associated with the increased synthesis of phosphatidylcholine and a reduced phosphatidylethanolamine/phosphatidylcholine ratio in the ER of *ups1*Δ cells which suppresses the UPR. Moreover, we observed inhibition of target of rapamycin complex 1 (TORC1) signaling in these cells. Activation of either UPR by ER protein stress or of TORC1 signaling by disruption of its negative regulator, the Seh1-associated complex inhibiting TORC1 complex, increased cytosolic protein synthesis, and restored glycolytic growth of *ups1*Δ cells. These results demonstrate that PA influx into mitochondria is required to preserve ER membrane homeostasis and that its disturbance is associated with impaired glycolytic growth and cellular stress signaling.

The functional integrity of mitochondria depends on characteristic lipid compositions of their membranes, the mitochondrial outer and inner membrane (OM and IM) (1, 2). This is exemplified by the hallmark lipid of mitochondria, cardiolipin (CL), which is pivotal for the structure and function of mitochondria. CL maintains respiration and cristae morphogenesis, ensures protein biogenesis and affects the fusion and fission of mitochondrial membranes (3–6). Altered CL levels in the OM modulate mitophagy and apoptosis (7–11). Hence, reduced levels and aberrant acylation or peroxidation of CL compromise mitochondrial activities and are associated with aging and various pathophysiological conditions, including cardiomyopathies, skeletal myopathies, ataxias, or nonalcoholic fatty liver disease (12–15).

CL is synthesized along an enzymatic cascade at the IM from phosphatidic acid (PA), which is mainly synthesized in the endoplasmic reticulum (ER) and imported into mitochondria (16). Although it has been reported that PA can be produced in mitochondrial membranes by phospholipases and kinases (17, 18), the maintenance of mitochondrial lipid homeostasis requires extensive exchange of phospholipids between the ER and mitochondria (19, 20). Similar to other membrane lipids, PA is transported from the ER to the OM at membrane contact sites, which facilitate the bi-directional transport of phospholipids between both organelles. Studies on the cellular distribution of newly synthesized phosphatidylserine (PS) revealed that phospholipid transfer to mitochondria can be driven by localized synthesis (21, 22). After reaching the OM, phospholipids are transported across the intermembrane space by conserved, lipid-specific lipid transfer proteins (23–28), which likely act in concert with MICOS membrane tethering complexes (24). Heterodimeric complexes of yeast Ups1 (human PRELID1) and Mdm35 (human TRIAP1) serve as PA-specific lipid transfer proteins (23, 26). Crystal structures of various members of the conserved Ups1/PRELID1 family of lipid transfer proteins show an internal lipid binding pocket, which is surrounded by a β-sheet and α-helices, reminiscent of other classes of lipid transfer proteins (29–32). Loss of Ups1 or PRELID1 in yeast or human cells, respectively, inhibits intramitochondrial PA transport and limits CL synthesis at the IM, which is accompanied by mitochondrial deficiencies, such as impaired respiration and mitochondrial fragmentation, and increases the susceptibility of the cells toward apoptotic stimuli (23, 26, 33–35).

High levels of PRELID1 and TRIAP1 were identified as an unfavorable prognostic marker in cancer (36). As cancer cells are often glycolytic, it is noteworthy that yeast cells lacking Ups1 also exhibit slow growth in glucose media (23, 34, 35). This phenotype is difficult to reconcile with reduced CL levels only, as cells lacking the CL synthase Crd1 in mitochondria

This article contains supporting information.

* For correspondence: Thomas Langer, TLanger@age.mpg.de.
Present address for Mari J. Aaltonen: Montreal Neurological Institute, McGill University, Montreal, Quebec, Canada.

grow normally in glucose-containing media although they are virtually devoid of CL (37). It therefore appears that the inhibition of intramitochondrial PA transport upon loss of Ups1 does not only perturb the mitochondrial membrane homeostasis but also causes deficiencies presumably beyond mitochondrial functions. Here, we demonstrate that a disturbed intramitochondrial transport of PA affects TORC1 signaling and alters the phospholipid homeostasis of the ER membrane modulating the unfolded protein response (UPR).

Results

The loss of Ups1 impairs basal UPR

To examine how the loss of Ups1 affects cell growth under glycolytic conditions, we used quantitative mass spectrometry (qMS) to determine the phospholipid profile of cellular membranes in wild-type and *ups1*Δ cells which were grown in glucose-containing media. In agreement with previous findings (23, 34), we observed reduced CL levels in *ups1*Δ cells, reflecting impaired PA transport to CL-synthesizing enzymes at the IM (Fig. 1, *A* and *B* and Fig. S1*A*). We also noted a significant increase of phosphatidylcholine (PC) and a decrease of phosphatidylethanolamine (PE), resulting in a low PE/PC ratio in cellular membranes (Fig. 1, *A*–*C* and Fig. S1*A*). Unexpectedly, deletion of *UPS1* also affected the phospholipid composition of ER membranes. We observed an increased total phospholipid content of an ER-enriched membrane fraction, which was accompanied by a significant increase of PC and phosphatidylinositol (PI) (Fig. 1, *D* and *E* and Fig. S1*B*), and a low PE/PC ratio (Fig. 1*F*).

Previous studies have reported that an increased PE/PC ratio in ER membranes activates the UPR independent of protein stress (38–41). We therefore monitored UPR induction in *ups1*Δ cells harboring GFP under the control of the UPR element (UPRE) in their genome (42). Whereas GFP accumulated in wild-type cells under basal conditions, GFP expression was decreased in cells lacking Ups1 which were grown in glucose- (Fig. 1, *G* and *H*) or galactose-containing media (Fig. S1, *C* and *D*). Moreover, we observed reduced mRNA levels of spliced *HAC1*, encoding a transcription factor involved in UPR (Fig. 1*I*) (43–45). We therefore conclude that basal gene expression under the control of UPRE is suppressed in *ups1*Δ cells. Notably and in contrast to *ups1*Δ cells, cells lacking other enzymes involved in CL synthesis (such as Tam41, Pgs1, or Crd1) did not show significant reduction of the GFP expression under UPRE (Fig. S1, *E*–*H*), pointing that CL defect per se does not lead to the suppression of UPR.

A central sensor of UPR is the ER kinase Ire1, which senses unfolded proteins in the ER lumen as well as lipid bilayer stress in the membrane (43, 46–48). To assess the contribution of lipid bilayer stress specifically, we exploited the previously described ΔIII mutant of Ire1, which is able to sense lipid bilayer stress but not unfolded ER proteins (49, 50). Cells expressing Ire1(ΔIII) recapitulated the suppression of the UPR by the loss of Ups1 (Fig. 1, *J* and *K*). These results suggest that the altered phospholipid composition of ER membranes limits UPR activation in *ups1*Δ cells.

Increased PC levels cause suppression of basal UPR

To examine how a decreased PE/PC ratio in ER membranes affects UPR, we induced *de novo* synthesis of PC via the Kennedy pathway by supplementing the growth medium with choline (51) and monitored UPR activity. Choline supplementation increased PC levels in ER-enriched membrane fractions of wild-type cells and led to a lower PE/PC ratio in these membranes (Fig. 2, *A* and *B*). Similar to cells lacking Ups1, the decreased PE/PC ratio in ER membranes was accompanied by an impaired basal UPR (Fig. 2, *C* and *D*), which was not altered in cells expressing mutant Ire1(ΔIII) (Fig. 2, *E* and *F*). We conclude from these experiments that the basal UPR is impaired if the PE/PC ratio in ER membranes is decreased, whereas an increased PE/PC ratio in ER membranes induces the UPR (41).

To unambiguously demonstrate that Ups1 affects UPR activation by modulating the phospholipid profile in ER membranes, we manipulated the PE/PC ratio in *ups1*Δ cells genetically. Yeast cells lacking Cho2 or Opi3, which are required for synthesis of PC from PE (51), accumulate PE relative to PC (Fig. 2*G*). Accordingly, deletion of *CHO2* or *OPI3* induces the UPR (41). We therefore deleted *CHO2* or *OPI3* in *ups1*Δ cells, which strongly increased the PE/PC ratio in an ER-enriched membrane fraction (Fig. 2, *G* and *H*). This was accompanied by UPR activation in the absence of Ups1 (Fig. 2, *I* and *J*). Thus, *ups1*Δ cells maintain the ability to induce the UPR upon lipid bilayer stress, but the reduced PE/PC ratio in the ER membrane of *ups1*Δ cells impairs the UPR under basal conditions.

UPR activation restores glycolytic growth of ups1Δ cells

Having established the link between Ups1 and UPR activation, we examined in further experiments whether the reduced UPR activity can explain the impaired glycolytic growth of *ups1*Δ cells. We therefore treated *ups1*Δ cells with tunicamycin, an inhibitor of protein glycosylation, which causes ER protein stress and induces the UPR. Treatment with tunicamycin activated the UPR both in wild-type and in *ups1*Δ cells (Fig. 3*A*) and allowed growth of *ups1*Δ cells on fermentable medium (Fig. 3*B*). Consistently, activation of the UPR upon overexpression of Ire1 (Fig. 3*C*) (47, 52) or deletion of *CHO2* or *OPI3* (Fig. 2, *I* and *J*) suppressed growth deficiencies of *ups1*Δ cells on glucose-containing medium (Fig. 3, *D* and *E*). The restoration of cell growth by tunicamycin and overexpression of Ire1 depended on Ire1-Hac1 signaling (Fig. 3, *F* and *G*), demonstrating that UPR activation is sufficient to promote glycolytic growth of *ups1*Δ cells. Notably, previous studies correlated the growth of *ups1*Δ cells on glucose-containing media with mitochondrial CL levels (53). However, overexpression of Ire1 did not alter the accumulation of CL (Fig. 3*G*). We therefore conclude that UPR activation is sufficient to allow growth of *ups1*Δ cells on fermentable carbon sources independent of CL levels in mitochondrial membranes.

Reduced cellular protein synthesis in ups1Δ cells

We noted that the loss of UPR activity in *ire1*Δ and *hac1*Δ cells did not limit growth in glucose-containing medium

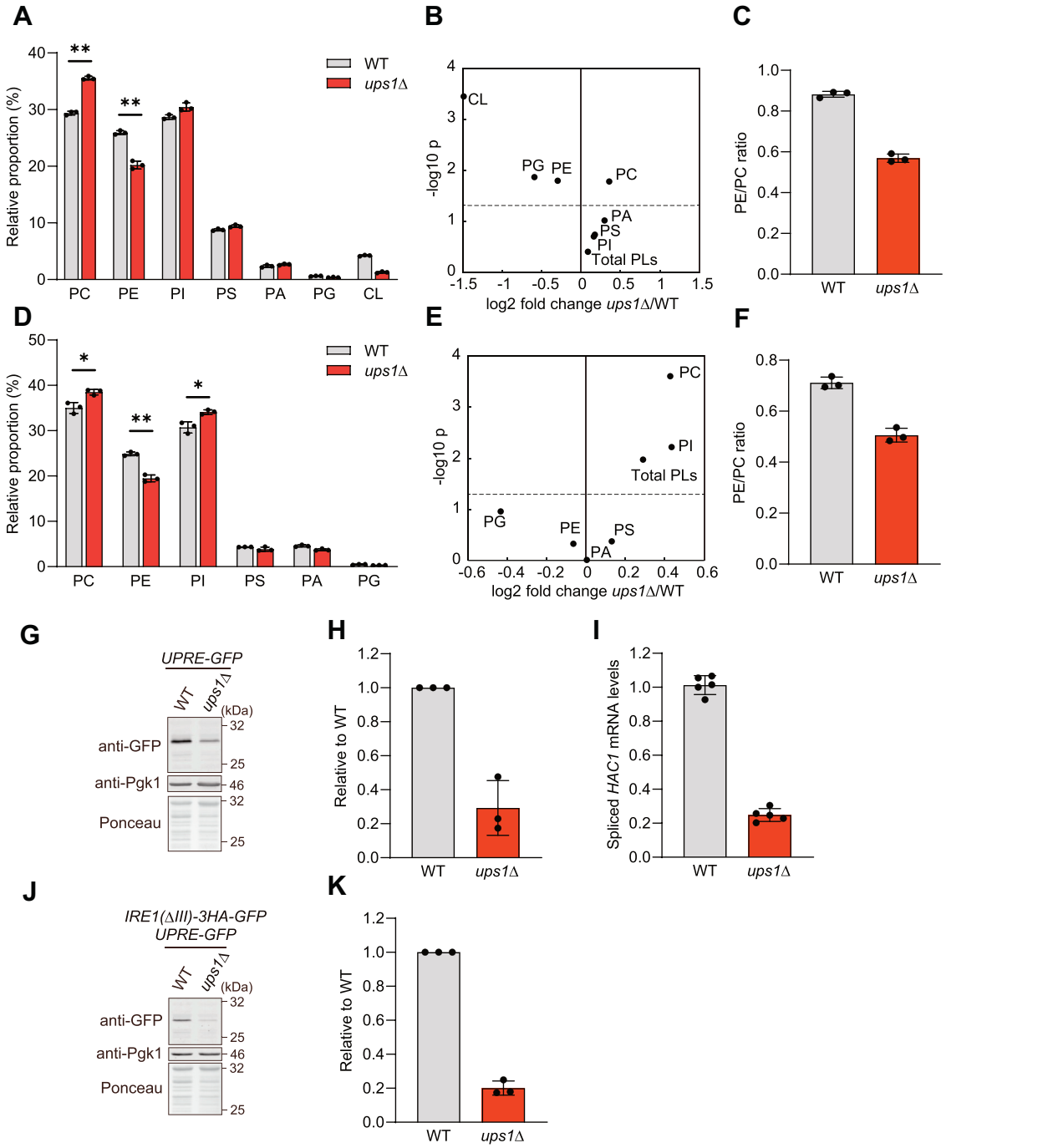

Figure 1. ER phospholipid composition is altered in *ups1*Δ cells. *A*, phospholipid composition in whole cell of wild-type (WT) and *ups1*Δ cells grown to log phase in SCD medium. Data represent mean ± SD (n = 3). $^{**}p < 0.01$. *B*, changes in the absolute abundance of phospholipids in whole cell of *ups1*Δ. Data represented as log2 fold change at *x*-axis with −log 10 *p* value of student's *t* test at *y*-axis. *Dashed line* represents $p = 0.05$. *C*, PE/PC ratio of WT and *ups1*Δ cells. *D*, phospholipid composition in ER-enriched microsome fraction from WT and *ups1*Δ cells grown to log phase in SCD medium. Data represent mean ± SD (n = 3). $^{*}p < 0.05$, $^{**}p < 0.01$. *E*, changes in the absolute abundance of phospholipids in ER-enriched microsome fraction of *ups1*Δ. Data represented as log2 fold change at *x*-axis with −log 10 *p* value of Student's *t* test at *y*-axis. *Dashed line* represents $p = 0.05$. *F*, PE/PC ratio in ER-enriched microsome fraction from WT and *ups1*Δ cells. *G*, WT and *ups1*Δ cells expressing *4xUPRE-GFP* grown to log phase in SCD medium were subjected to Western blotting. Pgk1 and ponceau staining were monitored as a loading control. *H*, GFP in (*G*) was quantified. GFP signals were normalized to Pgk1 and expressed relative to WT cells (set as one). Data represent mean ± SD (n = 3). *I*, WT and *ups1*Δ cells were grown to log phase in SCD medium. Spliced *HAC1* mRNA expression was analyzed by real time PCR and normalized to *ACT1* mRNA expression. Data represent mean ± SD (n = 5). *J*, WT and *ups1*Δ cells expressing Ire1(ΔIII)-3HA-GFP and *4xUPRE-GFP*grown to log phase in SCD medium were subjected to Western blotting. *K*, GFP in (*J*) was quantified as described in (*H*). Data represent mean ± SD (n = 3). ER, endoplasmic reticulum; PC, phosphatidylcholine; PE, phosphatidylethanolamine; SCD, synthetic complete glucose; UPRE, UPR element.

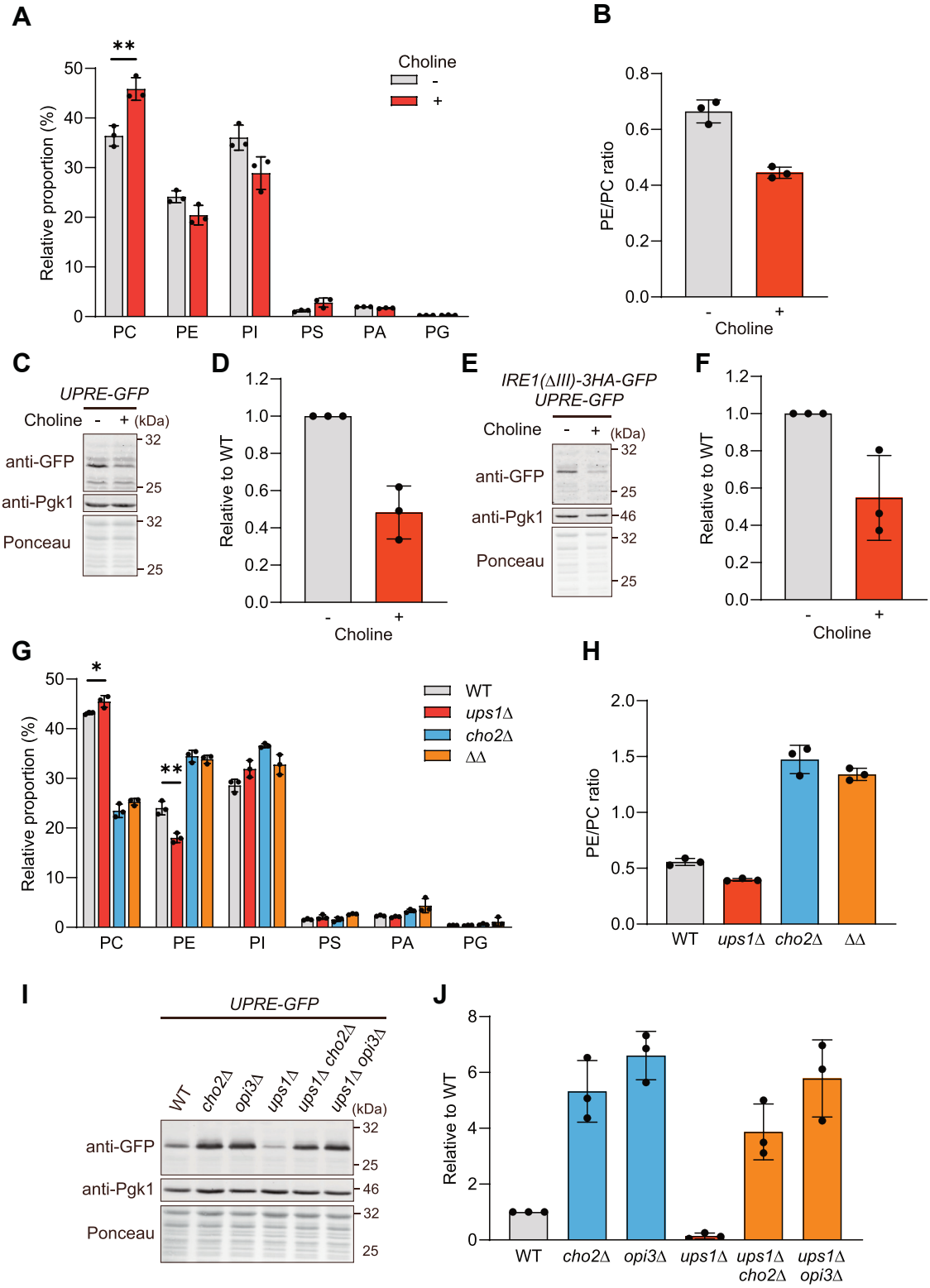

Figure 2. Basal UPR is suppressed in high PC levels. *A*, phospholipid composition in ER-enriched microsome fraction from wild-type (WT) cells grown to log phase in SCD medium with or without 1 mM choline. Data represent mean ± SD (n = 3). *B*, PE/PC ratio in ER-enriched microsome fraction from WT with or without choline. *C*, WT cells expressing *4xUPRE-GFP* grown to log phase in SCD medium with or without 1 mM choline were subjected to Western blotting. Pgk1 and ponceau staining were monitored as a loading control. *D*, GFP in (*C*) was quantified. GFP signals were normalized to Pgk1 and expressed relative to WT cells (set as one). Data represent mean ± SD (n = 3). *E*, WT cells expressing Ire1(ΔIII)-3HA-GFP and *4xUPRE-GFP* grown to log phase in SCD medium with or without 1 mM choline were subjected to Western blotting. *F*, GFP in (*E*) was quantified as described in (*D*). Data represent mean ± SD (n = 3). *G*, phospholipid composition in ER-enriched microsome fraction from WT, *ups1*Δ, *cho2*Δ and *ups1*Δ*cho2*Δ (ΔΔ) cells grown to log phase in SCD medium. Data represent mean ± SD (n = 3). *$p < 0.05$, **$p < 0.01$. *H*, PE/PC ratio of ER-enriched microsome fraction from WT, *ups1*Δ, *cho2*Δ and *ups1*Δ*cho2*Δ (ΔΔ) cells. *I*, WT, *cho2*Δ, *opi3*Δ, *ups1*Δ, *ups1*Δ*cho2*Δ, and *ups1*Δ*opi3*Δ cells expressing *4xUPRE-GFP* grown to log phase in SCD medium were subjected to Western blotting. *J*, GFP in (*I*) was quantified as described in (*D*). Data represent mean ± SD (n = 3). ER, endoplasmic reticulum; PC, phosphatidylcholine; PE, phosphatidylethanolamine; SCD, synthetic complete glucose; UPR, unfolded protein response; UPRE, UPR element.

(Fig. 3*F*). This contrasts *ups1*Δ cells and therefore points to additional deficiencies in *ups1*Δ cells that limit cell growth. We therefore determined transcriptome and proteome profiles of *ups1*Δ cells under glycolytic growth conditions (Tables S1 and S2). Consistent with the observed impaired UPR activity, canonical UPR target genes were expressed at lower levels in *ups1*Δ cells when compared with wild-type cells (Fig. S2*A*). Both transcriptome and proteome profiles pointed to reduced protein synthesis in *ups1*Δ cells (Fig. 4, *A* and *B*). The expression of genes involved in processes driving protein synthesis, such as rRNA processing or ribosome biogenesis, was most prominently downregulated in *ups1*Δ cells (Fig. 4*A* and Table S3). Consistently, proteins regulating rRNA processing accumulated at reduced levels in *ups1*Δ cells (Fig. 4*B* and Table S4). Together, these data demonstrate that protein synthesis is inhibited in Ups1-deficient cells. The expression of genes related to protein synthesis is decreased under stress conditions (54). Consistently, tunicamycin treatment limited the expression of genes involved in cellular protein synthesis (Fig. 4*C*). However, it partially promoted cellular protein synthesis in *ups1*Δ cells (Fig. 4*D* and Fig. S2*C*), consistent with the improved cell growth under these conditions (Fig. 3*B*).

TORC1 inhibition limits glycolytic growth of ups1Δ cells

The TORC1 regulates ribosome biogenesis in response to the metabolic status of cells (55). We noted an increased expression of genes coding core autophagy proteins in *ups1*Δ cells when compared with wild-type cells (Fig. S2*B* and Table S1), suggesting inhibition of TORC1 and induction of autophagy in *ups1*Δ cells. To directly assess TORC1 activity in *ups1*Δ cells, we monitored the level and phosphorylation of one of its substrates, Sch9 (56), an AGC family protein kinase, which is homologous to mammalian S6 and Akt kinases and regulates ribosome biogenesis (57, 58). We found that total Sch9 protein levels were not changed (Fig. 5, *A* and *B*), but Sch9 phosphorylation was significantly suppressed in *ups1*Δ cells compared with wild-type cells (Fig. 5, *C* and *D*). These results indicate low TORC1 activity in *ups1*Δ cells, which agrees with the reduced protein synthesis in these cells.

We hypothesized that, similar to UPR activity, an altered membrane lipid composition may inhibit TORC1 activity in *ups1*Δ cells. However, neither loss of the CL synthase Crd1 to decrease CL levels (Fig. S3*A*) nor choline supplementation of wild-type cells to mimic the PE/PC ratio of *ups1*Δ cells affected TORC1 activity and phosphorylation of Sch9 (Fig. S3, *B*–*E*). Similarly, decreased PE levels upon loss of the mitochondrial PS transfer protein Ups2 did not alter TORC1 activity (Fig. S3, *B* and *C*). TORC1 activity is dependent on PA (59, 60), but disturbed intramitochondrial PA transport in *ups1*Δ cells did not result in the accumulation of PA in ER-enriched membrane fractions (Fig. 1, *D* and *E*). Moreover, PA accumulation upon inhibition of the PA phosphatase in *nem1*Δ or *spo7*Δ cells did not affect Sch9 phosphorylation (Fig. S3, *F* and *G*). Thus, other deficiencies appear to inhibit TORC1 activity in *ups1*Δ cells.

To examine whether TORC1 inhibition limits the glycolytic growth of *ups1*Δ cells, we used a genetic approach. The Seh1-associated complex inhibiting TORC1 consisting of Npr2, Npr3, and Iml1 functions as negative regulator of TORC1 in yeast (61, 62). Constitutive activation of TORC1 upon deletion of one of the Seh1-associated complex inhibiting TORC1 subunits restored cell growth of *ups1*Δ cells (Fig. 5, *E* and *F*). Moreover, expression of a phosphomimetic mutant variant of Sch9, Sch9^{2D3E}, greatly restored the growth of *ups1*Δ (Fig. 5*G*). We therefore conclude that inhibition of TORC1-Sch9 signaling impairs the growth of *ups1*Δ cells on a fermentable carbon source such as glucose. Notably, TORC1 activation upon expression of Sch9^{2D3E} in *ups1*Δ cells did not restore UPR activity (Fig. 5, *H* and *I*), indicating that both pathways promote glycolytic growth of *ups1*Δ cells independently.

Discussion

Ups1-dependent transport of PA to the IM promotes CL synthesis (23). Here, we have unraveled an unexpected link between intramitochondrial PA transport and cellular signaling (Fig. 6). Disturbed PA transport in mitochondria lacking Ups1 limits the activation of UPR and inhibits TORC1. TORC1 signaling controls ribosome biogenesis and protein synthesis, which is suppressed in *ups1*Δ cells and limits glycolytic cell growth. Accordingly, activation of either UPR or TORC1 is sufficient to suppress growth deficiencies in the absence of Ups1. Thus, the flux of PA into mitochondria does not only ensure mitochondrial CL synthesis and membrane biogenesis but is coupled to the phospholipid homeostasis of other cellular membranes affecting cell signaling.

Several lines of evidences reveal that the disturbed intramitochondrial PA transport in *ups1*Δ cells impairs independently CL synthesis and UPR and TORC1 signaling. The activation of the UPR allowed glycolytic growth of *ups1*Δ cells but did not restore the accumulation of CL in mitochondrial membranes (Fig. 3*G*) or the phosphorylation of Sch9 (Fig. 5, *C* and *D*). On the other hand, mimicking the PE/PC ratio observed in *ups1*Δ cells by choline supplementation of wild-type cells suppressed UPR but did not alter the phosphorylation of Sch9 (Fig. S3, *D* and *E*). Conversely, expression of phosphomimetic Sch9^{2D3E} mutant did not restore basal UPR in *ups1*Δ cells (Fig. 5, *H* and *I*). These findings are consistent with a previous study demonstrating that activation of TORC1 does not affect the UPR (63). Moreover, CL deficiencies in cells lacking the CL synthase Crd1 did not suppress TORC1 signaling (Fig. S3, *B* and *C*) or basal UPR (Fig. S1, *E* and *F*). Therefore, we conclude that the impaired intramitochondrial PA transport rather than the CL deficiency leads to the alteration of stress signaling cascades outside of *ups1*Δ mitochondria.

Inhibition of PA transport across the intermembrane space in *ups1*Δ cells is associated with an increased PC and PI and a decreased PE/PC ratio but not with a significant accumulation of PA in the ER membrane. This indicates efficient bi-directional transport of PA between the OM and the ER membrane and suggests that PA is rapidly metabolized in the ER, if it is not consumed for CL synthesis in *ups1*Δ mitochondria. Because PA serves as a common precursor for the synthesis of PC and CL, PA is likely converted to PC resulting

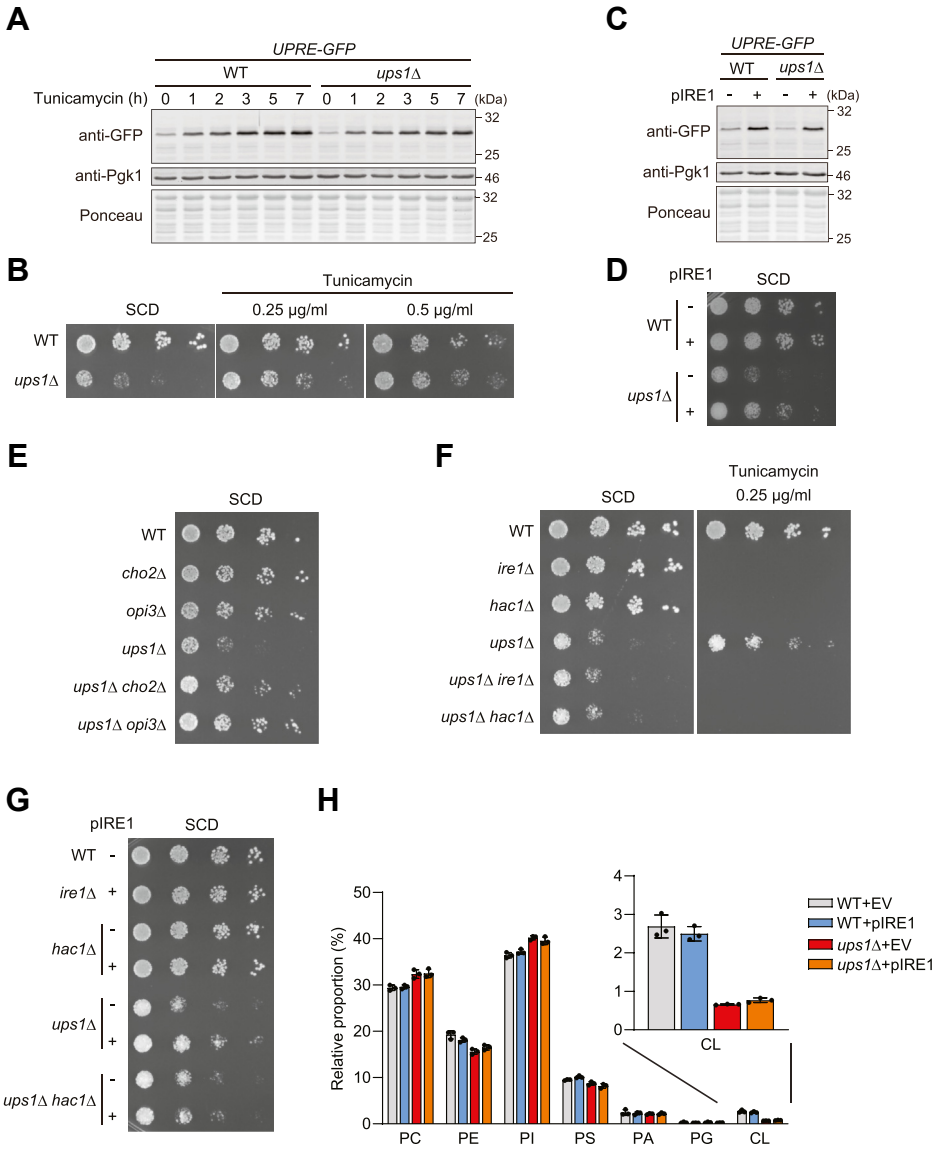

Figure 3. Glycolytic growth of *ups1*Δ cells is restored upon UPR activation. *A*, wild-type (WT) and *ups1*Δ cells expressing *4xUPRE-GFP* grown to log phase in SCD medium were treated with 1 μg/ml tunicamycin, collected at the indicated time points, and subjected to Western blotting. Pgk1 and ponceau staining were monitored as a loading control. *B*, serial dilutions of WT and *ups1*Δ cells were spotted on SCD medium with or without tunicamycin (concentration as 0.25 or 0.5 μg/ml) and incubated at 30 °C for 2 days (n = at least 3). *C*, *4xUPRE-GFP* expressing WT and *ups1*Δ cells transformed with an empty vector or a plasmid encoding Ire1 (pIRE1) were grown to log phase in SCD medium and subjected to Western blotting. *D*, serial dilutions of WT and *ups1*Δ cells transformed with an empty vector or pIRE1 were spotted on SCD medium and incubated at 30 °C for 2 days (n = at least 3). *E*, serial dilutions of WT, *cho2*Δ, *opi3*Δ, *ups1*Δ, *ups1*Δ*cho2*Δ, and *ups1*Δ*opi3*Δ cells were spotted on SCD medium and incubated at 30 °C for 2 days (n = at least 3). *F*, serial dilutions of WT, *ire1*Δ, *hac1*Δ, *ups1*Δ, *ups1*Δ*ire1*Δ, *ups1*Δ*hac1*Δ cells were spotted on SCD medium with or without 0.25 μg/ml tunicamycin and incubated at 30 °C for 2 days (n = at least 3). *G*, serial dilutions of WT, *ire1*Δ, *hac1*Δ, *ups1*Δ, *ups1*Δ*hac1*Δ cells transformed with an empty vector or pIRE1 were spotted on SCD medium and incubated at 30 °C for 2 days (n = 3). *H*, phospholipid composition in whole cell of WT and *ups1*Δ cells transformed with an empty vector or pIRE1. Data represent mean ± SD (n = 3). SCD, synthetic complete glucose; UPR, unfolded protein response; UPRE, UPR element.

in lowered PE/PC ratios in the ER membrane and the inhibition of UPR. Rapid conversion to PC can also explain why impaired PA utilization in mitochondria does not suppress Opi1, the transcriptional repressor of phospholipid synthesis, which is regulated by PA (51). Transcript profiling revealed no increased expression of Opi1 target genes in *ups1*Δ cells, consistent with the unaltered PA levels and increased PI in ER membranes in *ups1*Δ cells. The uncontrolled accumulation of PC and PI in the ER membrane may also retard functionality of the ER in addition to the limited UPR activation, contributing to the impaired glycolytic growth in *ups1*Δ cells.

The low PE/PC ratio in ER membranes suppresses the basal UPR in *ups1*Δ cells, complementing previous findings which revealed UPR activation upon an increase of the PE/PC ratio (41). The ratio of PE and PC determines membrane packing and curvature stress in the ER membrane, which appears to be sensed by the Ire1 kinase. Indeed, an amphipathic helix adjacent to the transmembrane domain of Ire1 was found to detect biophysical changes at the ER membrane (64). It therefore can be envisioned that the low PE/PC ratio may improve membrane packing and restrain the formation of the X-shaped transmembrane dimer of Ire1.

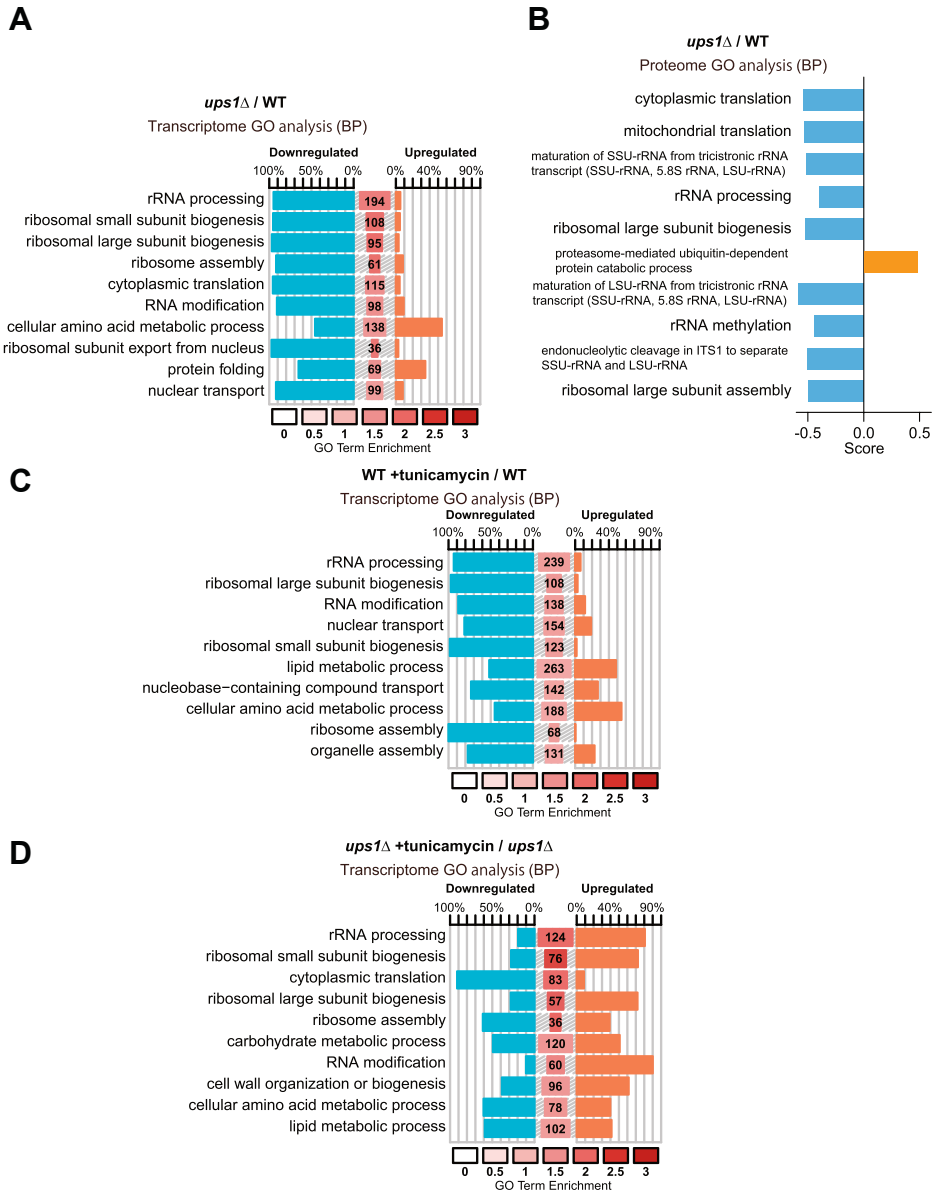

Figure 4. *ups1*Δ cells show suppressed ribosome synthesis. *A*, symplot representing the changed genes within an enriched biological process (BP) GO terms in *ups1*Δ cells against wild-type (WT) cells. Top ten significant terms from yeast GO-slim are plotted. Percentage of downregulated (*blue*) and upregulated (*red*) genes in each term is shown. The size of the central bars was directly proportional to the number of genes in the query belonging to the respective term, and the enrichment value is represented by the color of the bar as previously reported (71). *B*, 1D annotation enrichment analysis of proteome in *ups1*Δ cells against WT cells is shown. Annotation is biological process (BP) GO terms (76). Score represents difference of the distribution of the ratios for the proteins corresponding to GO terms from the ratios of the distribution for all proteins. Top ten significant terms are indicated. *C*, symplot representing the changed genes within a BP GO terms in WT cells treated with 1 μg/ml tunicamycin for 3 h against non-treated WT cells. Top ten significant terms from Yeast GO-slim are plotted. *D*, symplot representing the changed genes within an enriched BP GO terms in *ups1*Δ cells treated with 1 μg/ml tunicamycin for 3 h against nontreated *ups1*Δ cells. Top ten significant terms from yeast GO-slim are plotted. GO, Gene Ontology.

Protein synthesis is suppressed under stress conditions (54). Our transcriptome data correspondingly show that expression levels of genes involved in ribosome biogenesis are decreased in wild-type cells treated with tunicamycin. On the other hand, tunicamycin induces a number of those genes in *ups1*Δ cells in accordance with the recovery of glycolytic growth of the cells. One remaining question is how tunicamycin treatment induces genes involved in protein synthesis, although it does not restore TORC1 signaling in *ups1*Δ cells. In contrast to the previous indication that the suppression of protein synthesis with tunicamycin proceeds independent of the UPR (65), the growth recovery of *ups1*Δ cells by tunicamycin depends on Ire1 and Hac1. Therefore, our results imply the existence of an UPR-dependent pathway promoting protein synthesis that is induced by proteotoxic stress in *ups1*Δ cells.

The loss of Ups1 also impairs TORC1 signaling independent of UPR inhibition. TORC1 inhibition in *ups1*Δ cells is not caused by alterations in the membrane lipid composition of the ER membrane, as neither a decreased PE/PC ratio, nor the accumulation of PA by other means (*e.g.*, inhibition of PA phosphatase complex in *nem1*Δ or *spo7*Δ cells; Fig. S3, *F* and *G*) resulted in the inhibition of TORC1 activity. Notably,

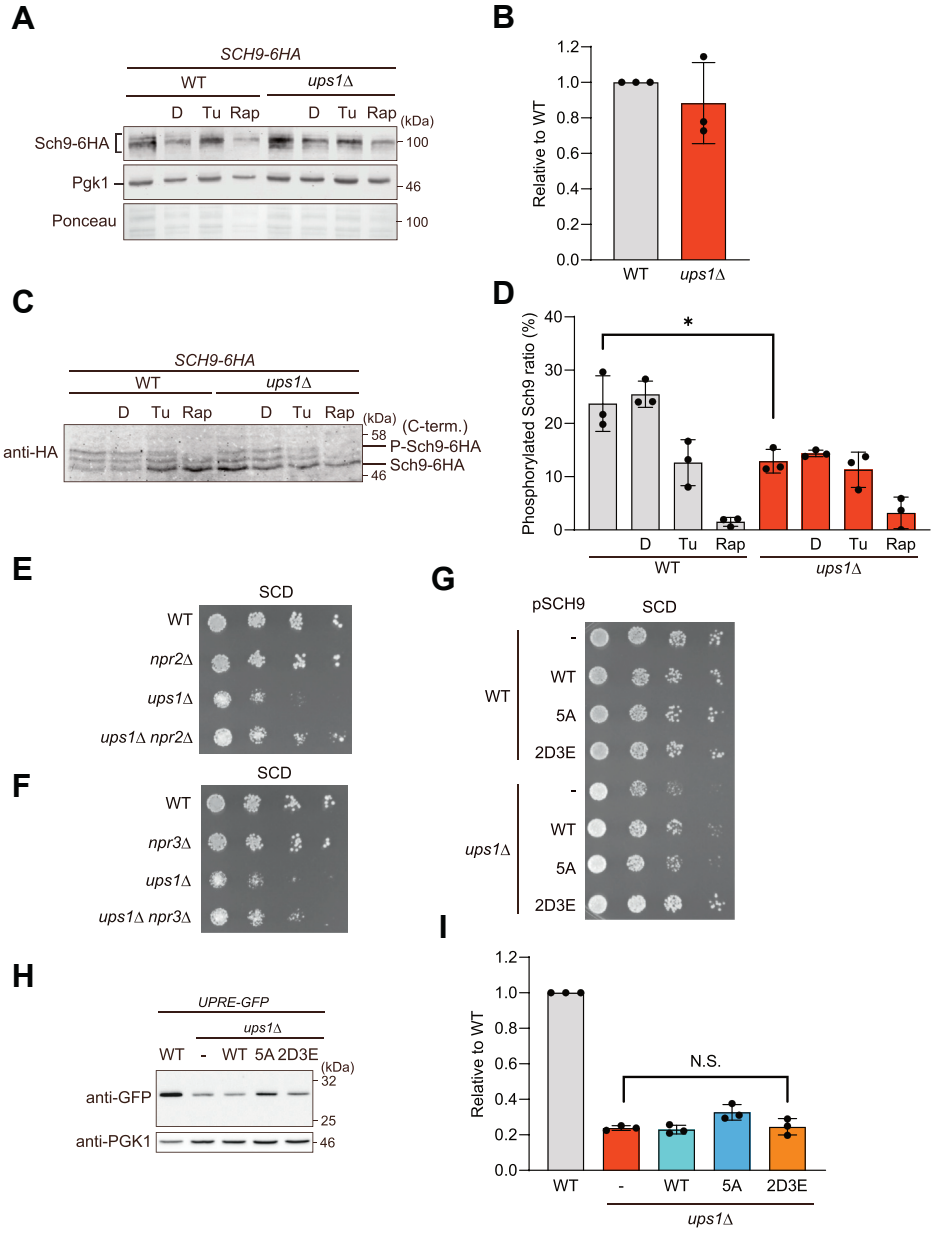

Figure 5. TORC1-Sch9 signaling is impaired in *ups1Δ* cells. *A*, wild-type (WT) and *ups1*Δ cells expressing Sch9-6HA grown to log phase in SCD medium were treated with DMSO (*D*), 1 μg/ml tunicamycin (Tu), or 0.2 μg/ml rapamycin (Rap) for 3 h and subjected to Western blotting. Pgk1 and ponceau staining were monitored as a loading control. *B*, Sch9-6HA of nontreated cells in (*A*) was quantified. Total Sch9-6HA signals were normalized to Pgk1 and expressed relative to wild-type cells (set as one). Data are means ± SD (n = 3). *C*, WT and *ups1*Δ cells expressing Sch9-6HA grown to log phase in SCD medium were treated with DMSO (*D*), 1 μg/ml tunicmycin (Tu), or 0.2 μg/ml rapamycin (Rap) for 3 h. For the analysis of Sch9 phosphorylation, lysates were treated with NTCB and subjected to Western blotting. *D*, Phosphorylated Sch9-6HA ratio in (*C*) was quantified. Phosphorylated Sch9-6HA signals were divided with total Sch9-6HA signals. Data represent mean ± SD (n = 3). *$p < 0.05$. *E*, Serial dilutions of WT, *npr2*Δ, *ups1*Δ, and *ups1*Δ*npr2*Δ cells were spotted on SCD medium and incubated at 30 °C for 2 days (n = 3). *F*, Serial dilutions of WT, *npr3*Δ, *ups1*Δ, and *ups1*Δ*npr3*Δ cells were spotted on SCD medium and incubated at 30 °C for 2 days (n = 3). *G*, Serial dilutions of WT and *ups1*Δ cells transformed with an empty vector or a plasmid encoding $Sch9^{WT}$ (pSCH9), $Sch9^{5A}$ (T723A, S726A, T737A, S758A, S765A), or $Sch9^{2D3E}$ (T723D, S726D, T737E, S758E, S765E) were spotted on SCD medium and incubated at 30 °C for 2 days (n = at least 3). *H*, *4xUPRE-GFP* expressing WT and *ups1*Δ cells transformed with an empty vector or a plasmid encoding $Sch9^{WT}$, $Sch9^{5A}$, or $Sch9^{2D3E}$ were grown to log phase in SCD medium and subjected to Western blotting. *I*, GFP in (*H*) was quantified. GFP signals were normalized to Pgk1 and expressed relative to WT cells (set as one). Data represent mean ± SD (n = 3). N.S., not significant; NTCB, 2-nitro-5-thiocyanobenzoic acid; SCD, synthetic complete glucose; UPRE, UPR element.

previous studies have reported that TORC1-dependent Sch9 phosphorylation is inhibited by mitochondrial depolarization (66), coupling mitochondrial OXPHOS activity with cellular nutrient signaling. Because mitochondrial membrane potential is low in *ups1*Δ cells grown in glucose media (35), it is conceivable that mitochondrial depolarization upon inhibition of PA transport interferes with TORC1 signaling in *ups1*Δ cells. Interestingly, the strong induction of Pdr3, Pdr5, and Pdr15 in *ups1*Δ cells suggests induction of the mitochondrial compromised protein import response (67), which is in line with mitochondrial depolarization and import defects in *ups1*Δ cells (35). Therefore, it is tempting to speculate that signaling cascades in response to mitochondrial protein import stress might contribute to the TORC1 inhibition in *ups1*Δ cells

(68). While further studies are needed to elucidate the link between mitochondrial depolarization and TORC1 signaling, our findings highlight that disturbances in the intra-mitochondrial transport of phospholipids and alterations in the phospholipid composition of mitochondrial membranes can broadly affect cellular signaling.

Experimental procedures

Yeast strains

Saccharomyces cerevisiae strains used in this study are based on S288c or W303. The genotype of the yeast strains is described in the strain list table (Table S5). Genes were deleted by PCR-targeted homologous recombination with the respective forward and reverse primers. Plasmids encoding disruption maker, HphNT1, NatNT2 or KanMX6, were used as template. C-terminal 6xHA tag of Sch9 at its endogenous loci was constructed using PCR-targeted homologous recombination with plasmid encoding 6HA-NatNT2 (69). For construction of cells expressing both Ire1(ΔIII)-3HA-GFP and *4xUPRE-GFP*, *4xUPRE-GFP* was integrated by PCR-targeted homologous recombination at the *URA3* locus in cells expressing Ire1(ΔIII)-3HA-GFP kindly provided by R. Ernst (PZMS, Homburg). *4xUPRE-GFP-URA3* was amplified using as a template genomic DNA of a yeast strain, which contained this gene and which was kindly provided by M. Graef (MPI aging, Cologne) as a template.

Growth conditions

Yeast strains were cultured in YPD medium (1% yeast extract, 2% peptone, and 2% glucose) or synthetic complete glucose (SCD) medium (0.17% yeast nitrogen base without amino acids, ammonium sulfate, 0.5% ammonium sulfate, and 2% glucose) supplemented with necessary amino acids at 30 °C. Choline (1 mM; SIGMA) in water, tunicamycin (0.25, 0.5 or 1 μg/ml; Merck) in DMSO or rapamycin (0.2 μg/ml; SIGMA) in DMSO were added to the media when indicated. For cell growth assay, cells were grown in SCD plate for 1 day at 30 °C and suspended in water at a concentration of 0.1 OD_{600} units. Four microliter of 5-fold serial dilutions of cells were spotted on SCD plates and incubated for 2 days at 30 °C.

Preparation of ER-enriched microsomes

Hundred OD_{600} units of cells grown to log phase in SCD medium were collected by centrifugation (3000*g*, 5 min), washed once with H_2O, resuspended in Tris-DTT buffer (0.1 M Tris, 10 mM DTT), and incubated for 15 min at 30 °C. Cells were collected by centrifugation (3000*g*, 5 min), washed once with 1.2 M sorbitol, resuspended in sorbitol-phosphate buffer (20 mM potassium phosphate buffer [pH 7.4], 1.2 M sorbitol) containing lyticase, and incubated for 40 min at 30 °C. Spheroplasts were collected by centrifugation (3000*g*, 5 min) and resuspended in ice-cold homogenization buffer (0.6 M sorbitol, 10 mM Tris-HCl [pH 7.4], 1 mM EDTA, 0.3% BSA [fatty acid free], 1 mM PMSF). Whole cell homogenates were subjected to centrifugation (1200*g*, 5 min, 4 °C). Membrane and microsomes soluble fraction were separated by centrifugation (17,500*g*, 5 min, 4 °C). Supernatant was transferred to new tubes and subjected to centrifugation (40,000*g*, 40 min, 4 °C). The pellet was resuspended in 200 μl of pure water, and the protein concentration was determined by BCA assay. Aliquots of 50 μg protein were kept at −80 °C and were subjected to lipid analysis by qMS.

Quantitative mass spectrometry of phospholipids

0.5 OD_{600} unit of cells or 5 μg protein of ER-enriched microsomes were used for lipid analysis by qMS. Mass-spectrometric analysis of phospholipids was performed essentially as described (70). Briefly, lipids were extracted from samples in the presence of internal standards of major phospholipids (PC 17:0–14:1, PE 17:0–14:1, PI 17:0–14:1, PS 17:0–14:1, PA 17:0–14:1, PG 17:0–14:1 all from Avanti Polar Lipids) and CL

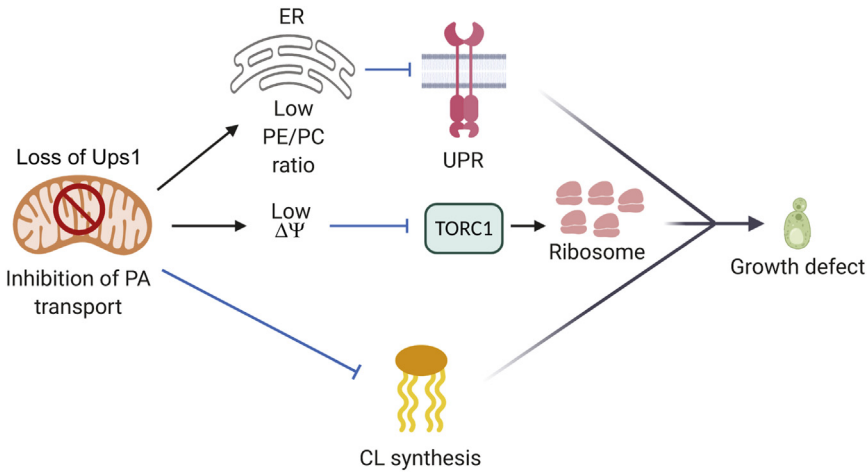

Figure 6. Altered PA transport in mitochondria affects UPR activation and TORC1 signaling. Impaired PA transport in mitochondria upon loss of Ups1 alters the ER lipid composition (low PE/PC ratio) inhibiting UPR. Independently, TORC1-Sch9 signaling is suppressed in *ups1*Δ cells. Deficiencies in UPR and TORC1 signaling combined with reduced CL synthesis limit cell growth. CL, cardiolipin; ER, endoplasmic reticulum; PA, phosphatidic acid; PC, phosphatidylcholine; PE, phosphatidylethanolamine; TORC1, target of rapamycin complex 1; UPR, unfolded protein response.

(CL mix I, Avanti Polar Lipids LM-6003). Extraction was performed according to Bligh and Dyer with modifications. Final lipid samples were dissolved in 10 mM ammonium acetate in methanol and were sprayed into a QTRAP 6500 triple quadrupole mass spectrometer (SCIEX) by nanoinfusion spray device (TriVersa NanoMate with ESI-Chip type A, Advion). The quadrupoles Q1 and Q3 were operated at unit resolution. Phospholipid analysis was carried out in positive ion mode. PC analysis was carried out by scanning for precursors of m/z 184 at a collision energy (CE) of 37 eV. PE, PI, PS, PG, and PA measurements were performed by scanning for neutral losses of 141, 277, 185, 189, and 115 Da at CEs of 30, 30, 30, 25, and 25 eV, respectively. CL species were identified by scanning for precursors of the masses (m/z 465.4, 467.4, 491.4, 493.4, 495.4, 505.5, 519.5, 521.5, 523.5, 535.5, 547.5, 549.5, 551.5, 573.5, 575.5, 577.5, 579.5, 601.5, 603.5, 605.5, 607.5, 631.5, 715.5, and 771.5 Da) corresponding DAG-H_2O fragments as singly charged ions at CEs of 45 eV. Mass spectra were analyzed by the LipidView Software Version 1.2 (SCIEX) for identification, correction of isotopic overlap, and quantification of lipids. Correction of isotopic overlap in CL species was performed using a spreadsheet calculating and subtracting theoretical amounts of [M + 2] and [M + 4] isotopes of each CL species that are isobalic to other CL species. Lipid amounts (pmol) were corrected for response differences between internal standards and endogenous lipids.

Immunoblotting

One OD_{600} units of cells were collected, washed with H_2O, and extracted by alkaline lysis (0.24 M NaOH, 1% 2-mercaptoethanol, 1 mM PMSF). Protein was precipitated in 25% trichloroacetic acid for 10 min on ice. Precipitates were washed with ice-cold acetone two times, dried, resuspended in 50 µl protein sample buffer (60 mM Tris-HCl [pH 6.8], 2% SDS, 10% glycerol, 20 mM DTT, 0.025% bromophenol blue), and incubated for 20 min at 40 °C. Samples corresponding to 0.2 OD_{600} units of cells were separated by SDS-PAGE, immunobloted to nitrocellulose membrane, and immunodecorated with α-GFP (1:5000, ORIGENE), α-PGK1 (1:10,000, Abcam), or α-HA (1:1,000, Roche). Anti-rabbit, anti-mouse, or anti-rat secondary antibodies conjugated to Dylight 800 (1:40,000, LI-COR) were used and detected with the Odyssey Infrared Imaging System (LI-COR). Quantification of the signals was performed using Image Studio Lite (LI-COR).

RNA extraction and quantitative RT-PCR

Total RNA was isolated with the NucleoSpin RNA kit (MACHEREY-NAGEL) from 3 OD_{600} units of cells, according to the manufacturer's protocol. cDNA was synthesized with 1 µg RNA and the GoScript Reverse Transcription Mix, Oligo(dT) (Promega). Quantitative RT-PCR was performed with Power SYBR Green PCR Master Mix (Thermo Fisher Scientific) and the following primers: *ACT1* forward 5′-TGTCACCAACTGGGACGATA and reverse 5′-AACCAGCGTAAATTGGAACG; spliced *HAC1* forward 5′-GCGTAATCCAGAAGCGCAGT and reverse 5′-GTGATGAAGAAATCATTCAATTCAAATG. QuantStudio 5 (Thermo Fisher Scientific) was used for measurement. Data were analyzed according to the ΔΔCT method normalized to housekeeping gene *ACT1*.

RNA sequence for transcriptomics

Libraries were prepared using the Illumina TruSeq mRNA stranded sample preparation Kit. Library preparation started with 1 µg total RNA. After poly-A selection (using poly-T oligo-attached magnetic beads), mRNA was purified and fragmented using divalent cations under elevated temperature. The RNA fragments underwent reverse transcription using random primers. This is followed by second strand cDNA synthesis with DNA Polymerase I and RNase H. After end repair and A-tailing, indexing adapters were ligated. The products were then purified and amplified (14 PCR cycles) to create the final cDNA libraries. After library validation and quantification (Agilent tape station), equimolar amounts of library were pooled. The pool was quantified by using the Peqlab KAPA Library Quantification Kit and the Applied Biosystems 7900HT Sequence Detection System. The pool was sequenced with a PE100 run on a NovaSeq6000 sequencer.

Bioinformatics and data analysis for transcriptomics

Raw reads were quantified using the alignment-free quantification tool kallisto version 0.45.0. Reference genome is sacCer3. Gene counts were imported to R version 3.5.1 and normalized to library size using DESeq2 version 1.22.2. General differential gene expression was determined in pairwise comparisons using DESeq2. Functional enrichment of differentially expressed genes was performed using the DAVID API as previously reported (71). The Yeast Gene Ontology-slim list and information of gene function were obtained from the *Saccharomyces* Genome Database.

Protein lysis and digest for proteomics

One OD_{600} units of cells were lysed in 40 µl of 2% SDC in 100 mM Tris-HCl [pH 8.0], and lysate was cleared by centrifugation (12,000 rpm, 10 min, 25 °C). Supernatant was subjected to protein concentration determination. In total, 30 µg of protein were used for protein digestion. Proteins were reduced and alkylated by TCEP (10 mM) and CAA (20 mM) for 60 min at 45 °C. 1 µg of LysC endopeptidase was added and incubated at 37 °C or 2 h, followed by addition of 1 µg of Trypsin for digestion at 37 °C for 16 h. Digestion was stopped by addition of TFA to a final concentration of 0.5%. Lysates were cleared (SDC precipitates) by centrifugation, and the supernatant was subjected for desalting using the StageTip (material: SDB-RPS, Affinisep) technique (72).

To generate the peptide spectral library, 2 µl of each sample (all conditions pooled 1:1) was pooled and subjected to high pH reversed phase chromatography. The instrumentation consisted out of a ZirconiumTM Ultra HPLC and a PAL RTC autosampler. The buffer systems consisted out of two buffers. (A) 10 mM ammonium hydroxide and (B) 80% acetonitrile and 10 mM ammonium hydroxide. Peptides were separated according to their hydrophobicity using an in-house packed

column (length = 40 cm, inner diameter = 200 μm, 2.7-μm beads, PoroShell, Agilent Technologies) column. The instrument communicated and were controlled using the software Chronos (Axel Semrau GmbH). The gradient length was 60 min, and in total, 12 fractions were collected (1/60 s) and subsequently concentrated using a SpeedVac to complete dryness. Peptides were dissolved in 10 μl 2% formic acid, 2.5% acetonitrile of which 3 μl were injected per liquid chromatography and tandem mass spectrometry run.

Liquid chromatography and tandem mass spectrometry

For the MS/MS spectra library generation, the QExactive HF-x operated in a Top22 data-dependent mode. MS1 spectra were acquired in a mass range of 350 to 1750 m/z, using an AGC target of 3 × 106 and a resolution at 200 m/z of 60,000. MS/MS spectra were acquired at 15,000 resolution using an AGC target of 5 × 105 and a maximal injection time of 22 ms.

For data-independent acquisition measurements, MS1 spectra were acquired using a resolution of 60,000 and an AGC target of 1 × 106. For MS/MS independent spectra acquisition, 48 windows were acquired at an isolation m/z range of 15 Th and the isolation windows overlapped by 1 Th. The isolation center range covered a mass range of 385 to 1043 m/z. Fragmentation spectra were acquired at a resolution of 15,000 at 200 m/z using a maximal injection time of 22 ms and stepped normalized collision energies of 24, 27, 30. The default charge state was set to 4.

Bioinformatics and data analysis for proteomics

The MS/MS data-dependent spectra library was analyzed with MaxQuant 1.6.3.4 and the implemented Andromeda search engine (73) using default settings. The acquired MS2 spectra were correlated against the Uniprot reference Yeast proteome (downloaded 01.2019, 6007 entries). The maximum number of missed cleavages was set to 2. Carbamidomethylation at cysteine residues was defined as a fixed modification, whereas methionine oxidation and protein N-terminal acetylation were defined as variable modification. The false discovery rate (FDR) on the peptide spectrum match and protein level was estimated to 0.01 using the implemented decoy-based algorithm. The mass tolerance on the peptide precursor level to 20 ppm (first search) and 4.5 ppm (main search). On the fragment level (MS2), the mass tolerance was set to 20 ppm. The output txt folder was then used to build the spectral library in Spectronaut (v. 13.0.190604). Data-independent acquisition runs were analyzed using the following settings in Spectronaut (v. 14.10.201222) utilizing the DDA library. Acquired runs were aligned using Precision iRT algorithm in Spectronaut by applying nonlinear regression. The algorithm is based on correlation of extracted ion currents to a consensus elution profile (74). Mass tolerances were set as default (40 ppm for MS1 and MS2 level). Q-value cutoff on precursor and protein level was set to 0.01 using the implemented decoy method "mutated". A maximum of three precursors were picked per peptide. Quantification was done on the MS2 level using the are under curve. Protein identifications with single peptide identifications in the library were removed as well as proteins that were identified by a single library peptide in DDA runs.

The data were exported in pivot-table format and further processed in Perseus (75). For pairwise comparison a two-sided *t* test was utilized. The FDR was calculated by a permutation-based approach using 500 permutations and a fudge factor s0 of 0.1 A protein was considered to be significantly differently expressed at a FDR of 5%. No cutoff for the fold change was considered. 1D enrichments (76) were performed in Perseus software using the Gene Ontology annotations of the Uniprot database.

SCH9 phosphorylation assay

2-nitro-5-thiocyanobenzoic acid treatments were performed as previously reported with slight modifications (56). Ten OD_{600} units of cells were treated with 6% trichloroacetic acid for 5 min on ice, washed twice with ice-cold acetone, and dried using a SpeedVac. The pellets were re-dissolved in 150 μl of urea lysis buffer (50 mM Tris [pH 7.5], 5 mM EDTA, 6 M urea, 1% SDS, 1 mM PMSF, and 1× Protease/Phosphatase inhibitor cocktail (CST)) and lysed with 0.7-mm-diameter zirconia beads in beads beater (3 × 30 s). After incubation for 10 min at 65 °C and centrifugation (20,000*g*, 2 min), 100 μl of supernatant was transferred to a new 1.5 ml reaction tube. The lysates were mixed with 30 μl of 0.5 M CHES [pH 10.5] and 20 μl of 7.5 M 2-nitro-5-thiocyanobenzoic acid and incubated overnight at room temperature. Each sample was mixed with 50 μl of 4× protein sample buffer (240 mM Tris-HCl [pH 6.8], 8% SDS, 40% glycerol, 80 mM DTT, 0.1% bromophenol blue) and subjected to Western blotting.

Statistical analysis

Quantitative data are presented as arithmetic means ± standard deviation. The statistical significance in related figures was assessed using two-tailed Student's *t* test. A *p* values and the number of experiments (n) are described in corresponding figure legend.

Data availability

All data are contained within the manuscript. The mass spectrometry proteomics data have been deposited to the ProteomeXchange Consortium via the PRIDE partner repository (77) with the data set identifier: PXD022321. Transcriptomic data have been deposited to the GEO omnibus with the data set identifier GSE160861.

Acknowledgments—We are grateful to Martin Graef, Robert Ernst, and Robbie Loewith for the kind gifts of plasmids and yeast strains. We thank the Cologne Center for Genomics for performing RNA sequencing and the MPI aging bioinformatics facility for support in data processing. We also thank other lab members for discussion.

Author contributions—A. E., T. T., and T. L. conceived and designed the research. A. E. performed the majority of experiments and data

analysis. M. J. A generated strains and conducted initial analysis and growth assays. H. N. performed proteomic analysis. A. E., T. T., and T. L. wrote the manuscript.

Funding and additional information—This work was supported by JSPS Overseas Research Fellowships to A. E. and by grants of the Deutsche Forschungsgemeinschaft to T. T. (TA1132/2-1) and T. L. (LA918/14-1).

Conflict of interest—The authors declare that they have no conflicts of interest with the contents of this article.

Abbreviations—The abbreviations used are: CL, cardiolipin; ER, endoplasmic reticulum; IM, inner membrane; OM, outer membrane; PA, phosphatidic acid; PC, phosphatidylcholine; PE, phosphatidylethanolamine; PI, phosphatidylinositol; qMS, quantitative mass spectrometry; TORC1, target of rapamycin complex 1; UPR, unfolded protein response; UPRE, UPR element.

References

1. Tatsuta, T., and Langer, T. (2017) Intramitochondrial phospholipid trafficking. *Biochim. Biophys. Acta Mol. Cell Biol. Lipids* **1862**, 81–89
2. van Meer, G., Voelker, D. R., and Feigenson, G. W. (2008) Membrane lipids: Where they are and how they behave. *Nat. Rev. Mol. Cell Biol* **9**, 112–124
3. Paradies, G., Paradies, V., De Benedictis, V., Ruggiero, F. M., and Petrosillo, G. (2014) Functional role of cardiolipin in mitochondrial bioenergetics. *Biochim. Biophys. Acta* **1837**, 408–417
4. Musatov, A., and Sedlak, E. (2017) Role of cardiolipin in stability of integral membrane proteins. *Biochimie* **142**, 102–111
5. Ikon, N., and Ryan, R. O. (2017) Cardiolipin and mitochondrial cristae organization. *Biochim. Biophys. Acta Biomembr.* **1859**, 1156–1163
6. Kameoka, S., Adachi, Y., Okamoto, K., Iijima, M., and Sesaki, H. (2018) Phosphatidic acid and cardiolipin coordinate mitochondrial dynamics. *Trends Cell Biol.* **28**, 67–76
7. Pizzuto, M., and Pelegrin, P. (2020) Cardiolipin in immune signaling and cell death. *Trends Cell Biol.* **30**, 892–903
8. Bertero, E., Kutschka, I., Maack, C., and Dudek, J. (2020) Cardiolipin remodeling in Barth syndrome and other hereditary cardiomyopathies. *Biochim. Biophys. Acta Mol. Basis Dis.* **1866**, 165803
9. Chu, C. T., Ji, J., Dagda, R. K., Jiang, J. F., Tyurina, Y. Y., Kapralov, A. A., Tyurin, V. A., Yanamala, N., Shrivastava, I. H., Mohammadyani, D., Wang, K. Z. Q., Zhu, J., Klein-Seetharaman, J., Balasubramanian, K., Amoscato, A. A., *et al.* (2013) Cardiolipin externalization to the outer mitochondrial membrane acts as an elimination signal for mitophagy in neuronal cells. *Nat. Cell Biol.* **15**, 1197–1205
10. Lutter, M., Fang, M., Luo, X., Nishijima, M., Xie, X., and Wang, X. (2000) Cardiolipin provides specificity for targeting of tBid to mitochondria. *Nat. Cell Biol.* **2**, 754–761
11. Kuwana, T., Mackey, M. R., Perkins, G., Ellisman, M. H., Latterich, M., Schneiter, R., Green, D. R., and Newmeyer, D. D. (2002) Bid, Bax, and lipids cooperate to form supramolecular openings in the outer mitochondrial membrane. *Cell* **111**, 331–342
12. Claypool, S. M., and Koehler, C. M. (2012) The complexity of cardiolipin in health and disease. *Trends Biochem. Sci.* **37**, 32–41
13. Pollard, A. K., Ortori, C. A., Stoger, R., Barrett, D. A., and Chakrabarti, L. (2017) Mouse mitochondrial lipid composition is defined by age in brain and muscle. *Aging* **9**, 986–998
14. Peng, K. Y., Watt, M. J., Rensen, S., Greve, J. W., Huynh, K., Jayawardana, K. S., Meikle, P. J., and Meex, R. C. R. (2018) Mitochondrial dysfunction-related lipid changes occur in nonalcoholic fatty liver disease progression. *J. Lipid Res.* **59**, 1977–1986
15. Clarke, S. L., Bowron, A., Gonzalez, I. L., Groves, S. J., Newbury-Ecob, R., Clayton, N., Martin, R. P., Tsai-Goodman, B., Garratt, V., Ashworth, M., Bowen, V. M., McCurdy, K. R., Damin, M. K., Spencer, C. T., Toth, M. J., *et al.* (2013) Barth syndrome. *Orphanet J. Rare Dis.* **8**, 23
16. Lev, S. (2012) Nonvesicular lipid transfer from the endoplasmic reticulum. *Cold Spring Harb. Perspect. Biol.* **4**, a013300
17. Choi, S. Y., Huang, P., Jenkins, G. M., Chan, D. C., Schiller, J., and Frohman, M. A. (2006) A common lipid links Mfn-mediated mitochondrial fusion and SNARE-regulated exocytosis. *Nat. Cell Biol* **8**, 1255–1262
18. Bektas, M., Payne, S. G., Liu, H., Goparaju, S., Milstien, S., and Spiegel, S. (2005) A novel acylglycerol kinase that produces lysophosphatidic acid modulates cross talk with EGFR in prostate cancer cells. *J. Cell Biol.* **169**, 801–811
19. Osman, C., Voelker, D. R., and Langer, T. (2011) Making heads or tails of phospholipids in mitochondria. *J. Cell Biol* **192**, 7–16
20. Tamura, Y., Kawano, S., and Endo, T. (2020) Lipid homeostasis in mitochondria. *Biol. Chem.* **401**, 821–833
21. Gaigg, B., Simbeni, R., Hrastnik, C., Paltauf, F., and Daum, G. (1995) Characterization of a microsomal subfraction associated with mitochondria of the yeast, Saccharomyces cerevisiae. Involvement in synthesis and import of phospholipids into mitochondria. *Biochim. Biophys. Acta* **1234**, 214–220
22. Kannan, M., Lahiri, S., Liu, L. K., Choudhary, V., and Prinz, W. A. (2017) Phosphatidylserine synthesis at membrane contact sites promotes its transport out of the ER. *J. Lipid Res.* **58**, 553–562
23. Connerth, M., Tatsuta, T., Haag, M., Klecker, T., Westermann, B., and Langer, T. (2012) Intramitochondrial transport of phosphatidic acid in yeast by a lipid transfer protein. *Science* **338**, 815–818
24. Aaltonen, M. J., Friedman, J. R., Osman, C., Salin, B., di Rago, J. P., Nunnari, J., Langer, T., and Tatsuta, T. (2016) MICOS and phospholipid transfer by Ups2-Mdm35 organize membrane lipid synthesis in mitochondria. *J. Cell Biol.* **213**, 525–534
25. Miyata, N., Watanabe, Y., Tamura, Y., Endo, T., and Kuge, O. (2016) Phosphatidylserine transport by Ups2-Mdm35 in respiration-active mitochondria. *J. Cell Biol.* **214**, 77–88
26. Potting, C., Tatsuta, T., Konig, T., Haag, M., Wai, T., Aaltonen, M. J., and Langer, T. (2013) TRIAP1/PRELI complexes prevent apoptosis by mediating intramitochondrial transport of phosphatidic acid. *Cell Metab.* **18**, 287–295
27. MacVicar, T., Ohba, Y., Nolte, H., Mayer, F. C., Tatsuta, T., Sprenger, H. G., Lindner, B., Zhao, Y., Li, J., Bruns, C., Kruger, M., Habich, M., Riemer, J., Schwarzer, R., Pasparakis, M., *et al.* (2019) Lipid signalling drives proteolytic rewiring of mitochondria by YME1L. *Nature* **575**, 361–365
28. Saita, S., Tatsuta, T., Lampe, P. A., Konig, T., Ohba, Y., and Langer, T. (2018) PARL partitions the lipid transfer protein STARD7 between the cytosol and mitochondria. *EMBO J.* **37**, e97909
29. Watanabe, Y., Tamura, Y., Kawano, S., and Endo, T. (2015) Structural and mechanistic insights into phospholipid transfer by Ups1-Mdm35 in mitochondria. *Nat. Commun.* **6**, 7922
30. Miliara, X., Garnett, J. A., Tatsuta, T., Abid Ali, F., Baldie, H., Pérez-Dorado, I., Simpson, P., Yague, E., Langer, T., and Matthews, S. (2015) Structural insight into the TRIAP1/PRELI-like domain family of mitochondrial phospholipid transfer complexes. *EMBO Rep.* **16**, 824–835
31. Yu, F., He, F., Yao, H., Wang, C., Wang, J., Li, J., Qi, X., Xue, H., Ding, J., and Zhang, P. (2015) Structural basis of intramitochondrial phosphatidic acid transport mediated by Ups1-Mdm35 complex. *EMBO Rep.* **16**, 813–823
32. Miliara, X., Tatsuta, T., Berry, J. L., Rouse, S. L., Solak, K., Chorev, D. S., Wu, D., Robinson, C. V., Matthews, S., and Langer, T. (2019) Structural determinants of lipid specificity within Ups/PRELI lipid transfer proteins. *Nat. Commun.* **10**, 1130
33. Sesaki, H., Dunn, C. D., Iijima, M., Shepard, K. A., Yaffe, M. P., Machamer, C. E., and Jensen, R. E. (2006) Ups1p, a conserved intermembrane space protein, regulates mitochondrial shape and alternative topogenesis of Mgm1p. *J. Cell Biol* **173**, 651–658
34. Osman, C., Haag, M., Potting, C., Rodenfels, J., Dip, P. V., Wieland, F. T., Brugger, B., Westermann, B., and Langer, T. (2009) The genetic interactome of prohibitins: Coordinated control of cardiolipin and

phosphatidylethanolamine by conserved regulators in mitochondria. *J. Cell Biol.* **184**, 583–596
35. Tamura, Y., Endo, T., Iijima, M., and Sesaki, H. (2009) Ups1p and Ups2p antagonistically regulate cardiolipin metabolism in mitochondria. *J. Cell Biol.* **185**, 1029–1045
36. Uhlen, M., Zhang, C., Lee, S., Sjöstedt, E., Fagerberg, L., Bidkhori, G., Benfeitas, R., Arif, M., Liu, Z., Edfors, F., Sanli, K., von Feilitzen, K., Oksvold, P., Lundberg, E., Hober, S., *et al*. (2017) A pathology atlas of the human cancer transcriptome. *Science* **357**, eaan2507
37. Joshi, A. S., Thompson, M. N., Fei, N., Huttemann, M., and Greenberg, M. L. (2012) Cardiolipin and mitochondrial phosphatidylethanolamine have overlapping functions in mitochondrial fusion in Saccharomyces cerevisiae. *J. Biol. Chem.* **287**, 17589–17597
38. Gao, X., van der Veen, J. N., Vance, J. E., Thiesen, A., Vance, D. E., and Jacobs, R. L. (2015) Lack of phosphatidylethanolamine N-methyltransferase alters hepatic phospholipid composition and induces endoplasmic reticulum stress. *Biochim. Biophys. Acta* **1852**, 2689–2699
39. Fu, S., Yang, L., Li, P., Hofmann, O., Dicker, L., Hide, W., Lin, X., Watkins, S. M., Ivanov, A. R., and Hotamisligil, G. S. (2011) Aberrant lipid metabolism disrupts calcium homeostasis causing liver endoplasmic reticulum stress in obesity. *Nature* **473**, 528–531
40. Ho, N., Xu, C., and Thibault, G. (2018) From the unfolded protein response to metabolic diseases - lipids under the spotlight. *J. Cell Sci* **131**, jcs199307
41. Thibault, G., Shui, G., Kim, W., McAlister, G. C., Ismail, N., Gygi, S. P., Wenk, M. R., and Ng, D. T. (2012) The membrane stress response buffers lethal effects of lipid disequilibrium by reprogramming the protein homeostasis network. *Mol. Cell* **48**, 16–27
42. Pollard, M. G., Travers, K. J., and Weissman, J. S. (1998) Ero1p: A novel and ubiquitous protein with an essential role in oxidative protein folding in the endoplasmic reticulum. *Mol. Cell* **1**, 171–182
43. Walter, P., and Ron, D. (2011) The unfolded protein response: From stress pathway to homeostatic regulation. *Science* **334**, 1081–1086
44. Mori, K., Kawahara, T., Yoshida, H., Yanagi, H., and Yura, T. (1996) Signalling from endoplasmic reticulum to nucleus: Transcription factor with a basic-leucine zipper motif is required for the unfolded protein-response pathway. *Genes Cells* **1**, 803–817
45. Cox, J. S., and Walter, P. (1996) A novel mechanism for regulating activity of a transcription factor that controls the unfolded protein response. *Cell* **87**, 391–404
46. Cox, J. S., Shamu, C. E., and Walter, P. (1993) Transcriptional induction of genes encoding endoplasmic reticulum resident proteins requires a transmembrane protein kinase. *Cell* **73**, 1197–1206
47. Mori, K., Ma, W., Gething, M. J., and Sambrook, J. (1993) A transmembrane protein with a cdc2+/CDC28-related kinase activity is required for signaling from the ER to the nucleus. *Cell* **74**, 743–756
48. Credle, J. J., Finer-Moore, J. S., Papa, F. R., Stroud, R. M., and Walter, P. (2005) On the mechanism of sensing unfolded protein in the endoplasmic reticulum. *Proc. Natl. Acad. Sci. U. S. A.* **102**, 18773–18784
49. Kimata, Y., Ishiwata-Kimata, Y., Ito, T., Hirata, A., Suzuki, T., Oikawa, D., Takeuchi, M., and Kohno, K. (2007) Two regulatory steps of ER-stress sensor Ire1 involving its cluster formation and interaction with unfolded proteins. *J. Cell Biol.* **179**, 75–86
50. Promlek, T., Ishiwata-Kimata, Y., Shido, M., Sakuramoto, M., Kohno, K., and Kimata, Y. (2011) Membrane aberrancy and unfolded proteins activate the endoplasmic reticulum stress sensor Ire1 in different ways. *Mol. Biol. Cell* **22**, 3520–3532
51. Henry, S. A., Kohlwein, S. D., and Carman, G. M. (2012) Metabolism and regulation of glycerolipids in the yeast Saccharomyces cerevisiae. *Genetics* **190**, 317–349
52. Shamu, C. E., and Walter, P. (1996) Oligomerization and phosphorylation of the Ire1p kinase during intracellular signaling from the endoplasmic reticulum to the nucleus. *EMBO J.* **15**, 3028–3039
53. Miyata, N., Goda, N., Matsuo, K., Hoketsu, T., and Kuge, O. (2017) Cooperative function of Fmp30, Mdm31, and Mdm32 in Ups1-independent cardiolipin accumulation in the yeast Saccharomyces cerevisiae. *Sci. Rep.* **7**, 16447
54. Gasch, A. P., Spellman, P. T., Kao, C. M., Carmel-Harel, O., Eisen, M. B., Storz, G., Botstein, D., and Brown, P. O. (2000) Genomic expression programs in the response of yeast cells to environmental changes. *Mol. Biol. Cell* **11**, 4241–4257
55. Broach, J. R. (2012) Nutritional control of growth and development in yeast. *Genetics* **192**, 73–105
56. Urban, J., Soulard, A., Huber, A., Lippman, S., Mukhopadhyay, D., Deloche, O., Wanke, V., Anrather, D., Ammerer, G., Riezman, H., Broach, J. R., De Virgilio, C., Hall, M. N., and Loewith, R. (2007) Sch9 is a major target of TORC1 in Saccharomyces cerevisiae. *Mol. Cell* **26**, 663–674
57. Huber, A., French, S. L., Tekotte, H., Yerlikaya, S., Stahl, M., Perepelkina, M. P., Tyers, M., Rougemont, J., Beyer, A. L., and Loewith, R. (2011) Sch9 regulates ribosome biogenesis via Stb3, Dot6 and Tod6 and the histone deacetylase complex RPD3L. *EMBO J.* **30**, 3052–3064
58. Huber, A., Bodenmiller, B., Uotila, A., Stahl, M., Wanka, S., Gerrits, B., Aebersold, R., and Loewith, R. (2009) Characterization of the rapamycin-sensitive phosphoproteome reveals that Sch9 is a central coordinator of protein synthesis. *Genes Dev.* **23**, 1929–1943
59. Fang, Y., Vilella-Bach, M., Bachmann, R., Flanigan, A., and Chen, J. (2001) Phosphatidic acid-mediated mitogenic activation of mTOR signaling. *Science* **294**, 1942–1945
60. Foster, D. A. (2013) Phosphatidic acid and lipid-sensing by mTOR. *Trends Endocrinol. Metab.* **24**, 272–278
61. Dokudovskaya, S., and Rout, M. P. (2015) SEA you later alli-GATOR–a dynamic regulator of the TORC1 stress response pathway. *J. Cell Sci.* **128**, 2219–2228
62. Powis, K., and De Virgilio, C. (2016) Conserved regulators of Rag GTPases orchestrate amino acid-dependent TORC1 signaling. *Cell Discov.* **2**, 15049
63. Ahmed, K., Carter, D. E., and Lajoie, P. (2019) Hyperactive TORC1 sensitizes yeast cells to endoplasmic reticulum stress by compromising cell wall integrity. *FEBS Lett.* **593**, 1957–1973
64. Halbleib, K., Pesek, K., Covino, R., Hofbauer, H. F., Wunnicke, D., Hanelt, I., Hummer, G., and Ernst, R. (2017) Activation of the unfolded protein response by lipid bilayer stress. *Mol. Cell* **67**, 673–684 e678
65. Pincus, D., Aranda-Diaz, A., Zuleta, I. A., Walter, P., and El-Samad, H. (2014) Delayed Ras/PKA signaling augments the unfolded protein response. *Proc. Natl. Acad. Sci. U. S. A.* **111**, 14800–14805
66. Kawai, S., Urban, J., Piccolis, M., Panchaud, N., De Virgilio, C., and Loewith, R. (2011) Mitochondrial genomic dysfunction causes dephosphorylation of Sch9 in the yeast Saccharomyces cerevisiae. *Eukaryot. Cell* **10**, 1367–1369
67. Weidberg, H., and Amon, A. (2018) MitoCPR-A surveillance pathway that protects mitochondria in response to protein import stress. *Science* **360**, eaan4146
68. Samluk, L., Chroscicki, P., and Chacinska, A. (2018) Mitochondrial protein import stress and signaling. *Curr. Opin. Physiol.* **3**, 41–48
69. Janke, C., Magiera, M. M., Rathfelder, N., Taxis, C., Reber, S., Maekawa, H., Moreno-Borchart, A., Doenges, G., Schwob, E., Schiebel, E., and Knop, M. (2004) A versatile toolbox for PCR-based tagging of yeast genes: New fluorescent proteins, more markers and promoter substitution cassettes. *Yeast* **21**, 947–962
70. Tatsuta, T. (2017) Quantitative analysis of glycerophospholipids in mitochondria by mass spectrometry. *Methods Mol. Biol.* **1567**, 79–103
71. [preprint] Metge, F., Sehlke, R., and Boucas, J. (2018) AGEpy: A python package for computational biology. *bioRxiv*. https://doi.org/10.1101/450890
72. Rappsilber, J., Ishihama, Y., and Mann, M. (2003) Stop and go extraction tips for matrix-assisted laser desorption/ionization, nanoelectrospray, and LC/MS sample pretreatment in proteomics. *Anal. Chem.* **75**, 663–670
73. Cox, J., and Mann, M. (2008) MaxQuant enables high peptide identification rates, individualized p.p.b.-range mass accuracies and proteome-wide protein quantification. *Nat. Biotechnol.* **26**, 1367–1372
74. Bruderer, R., Bernhardt, O. M., Gandhi, T., Miladinović, S. M., Cheng, L. Y., Messner, S., Ehrenberger, T., Zanotelli, V., Butscheid, Y., Escher, C., Vitek, O., Rinner, O., and Reiter, L. (2015) Extending the limits of quantitative proteome profiling with data-independent acquisition and

application to acetaminophen-treated three-dimensional liver microtissues. *Mol. Cell. Proteomics* **14**, 1400–1410

75. Tyanova, S., Temu, T., and Cox, J. (2016) The MaxQuant computational platform for mass spectrometry-based shotgun proteomics. *Nat. Protoc.* **11**, 2301–2319
76. Cox, J., and Mann, M. (2012) 1D and 2D annotation enrichment: A statistical method integrating quantitative proteomics with complementary high-throughput data. *BMC Bioinformatics* **13 Suppl 16**, S12
77. Perez-Riverol, Y., Csordas, A., Bai, J., Bernal-Llinares, M., Hewapathirana, S., Kundu, D. J., Inuganti, A., Griss, J., Mayer, G., Eisenacher, M., Pérez, E., Uszkoreit, J., Pfeuffer, J., Sachsenberg, T., Yilmaz, S., *et al.* (2019) The PRIDE database and related tools and resources in 2019: Improving support for quantification data. *Nucleic Acids Res.* **47**, D442–d450